Biochimica et Biophysica Acta 1808 (2011) 154–163

Contents lists available at ScienceDirect

Biochimica et Biophysica Acta

journal homepage: www.elsevier.com/locate/bbamem

Mitoxantrone is expelled by the ABCG2 multidrug transporter directly from the plasma membrane

László Homolya [a,*], Tamás I. Orbán [a], László Csanády [b], Balázs Sarkadi [a]

[a] Membrane Biology Research Group, Semmelweis University, Hungarian Academy of Sciences, Diószegi u. 64, H-1113 Budapest, Hungary
[b] Department of Medical Biochemistry, Semmelweis University, Tűzoltó utca 37-47, H-1094 Budapest, Hungary

ARTICLE INFO

Article history:
Received 28 April 2010
Received in revised form 24 July 2010
Accepted 27 July 2010
Available online 4 August 2010

Keywords:
ABCG2
mitoxantrone
ABC transporter
multidrug resistance
transport kinetic model
hydrophobic vacuum cleaner

ABSTRACT

ABC multidrug transporter proteins expel a wide variety of structurally unrelated, mostly hydrophobic compounds from cells. The special role of these transporters both at the physiological barriers and in cancer cells is based on their extremely broad substrate recognition. Since hydrophobic compounds are known to partition into the lipid bilayer and accumulate in membranes, the "classical pump" model for the mechanism of multidrug transporter proteins has been challenged, and alternative models suggesting substrate recognition within the lipid bilayer have been proposed. Although much effort has been made to validate this concept, unambiguous evidence for direct drug extrusion from the plasma membrane has not been provided yet. Here we show a detailed on-line microscopic analysis of cellular extrusion of fluorescent anti-cancer drugs, mitoxantrone and pheophorbide A, by a key human multidrug transporter, ABCG2. Using the fully active GFP-tagged ABCG2 and exploiting the special character of mitoxantrone that gains fluorescence in the lipid environment, we were able to determine transporter-modulated drug concentrations separately in the plasma membrane and the intracellular compartments. Different kinetic models describing the various transport mechanisms were generated and the experimental data were analyzed using these models. On the basis of the kinetic analysis, drug extrusion from the cytoplasm can be excluded, thus, our results indicate that ABCG2 extrudes mitoxantrone directly from the plasma membrane.

1. Introduction

Human multidrug transporters, including MDR1, MRP1, and ABCG2, play crucial role in absorption, distribution, metabolism, excretion and toxicity of pharmacologically relevant drugs [1–5]. The medical importance of these transporters is even more evident in cancer therapy, since they significantly contribute to the clinical drug resistance, hindering the effectivity of chemotherapeutical regimens [6–10]. Both the physiological and pathophysiological roles of these transporters are based on their ability to expel an astonishingly wide variety of drugs from cells. Explaining this extremely broad substrate recognition remained a major challenge to the scientists for decades, even though a better understanding of the molecular mechanism of these transporters is crucial for the generation of structure-based specific drugs and modulators.

Similar to enzymes, most membrane transporter proteins specifically bind one or a limited number of substrates in a well-defined binding pocket. Following substrate recognition, transporter proteins translocate the transported substrate from one side to the other side of the membrane. However, this classical mechanism cannot be directly applied to the so-called multidrug transporters, which recognize an exceptionally large number of chemically unrelated compounds as substrates. In the early 1990s, special transport mechanisms were proposed to explain the "promiscuity" of these transporters. Since the transported substrates of the multidrug transporters are mostly lipophilic, the hypothetical models suggested less specific, hydrophobic substrate-transporter interaction within the lipid bilayer of the membrane. The "hydrophobic vacuum cleaner" model suggested direct extrusion of the drugs from the membrane lipid bilayer [11,12], whereas the "floppase" model proposed translocation of the substrate from the inner leaflet to the outer leaflet of the membrane resulting in a net cellular efflux [13]. Although the concept of hydrophobic substrate recognition seems to be rational, these proposals launched a long-lasting scientific debate, since only indirect experimental evidences supported the alternative models. Some experimental data indicated that ABC pumps are capable of extruding their substrates before they reach

Abbreviations: ABC transporter, ATP-binding cassette transporter; ABCG2, G2 multidrug transporter (breast cancer resistance protein, MXR/BCRP/ABCP); GFP, green fluorescent protein; GFP-G2, ABCG2 protein tagged with GFP; Ko143 or KO, specific inhibitor of ABCG2; MDR1, multidrug resistance transporter 1 (ABCB1, Pgp, P-glycoprotein); MRP1, multidrug resistance-associated protein (ABCC1); MX, Mitoxantrone; Pheo, Pheophorbide A; RMSE, Root Mean Square Error; ROI, Region of Interest

* Corresponding author. Tel.: +36 1 372 4317; fax: +36 1 372 4353.
E-mail addresses: homolya@biomembrane.hu (L. Homolya), orbant@biomembrane.hu (T.I. Orbán), laszlo.csanady@eok.sote.hu (L. Csanády), sarkadi@biomembrane.hu (B. Sarkadi).

0005-2736/$ – see front matter © 2010 Elsevier B.V. All rights reserved.
doi:10.1016/j.bbamem.2010.07.031

the cytosole [14–16]. Also, mapping the drug-binding sites to membrane-embedded part of the transporter [17–21] and a limited number of functional studies using reconstituted MDR1/Pgp [17,22,23] supported the idea of substrate recognition within the membrane.

Recently, we generated and expressed an N-terminally GFP-tagged version of ABCG2 (GFP-G2), and proved that this fusion protein is fully functional [24]. The transport activity of GFP-tagged ABCG2 has been demonstrated in various transport assays using radiolabeled drug substrate, methotrexate and the fluorescent dye, Hoechst 33342. The spectral separation in fluorescence techniques allows identifying subpopulation of cells expressing the transporter, and in parallel, monitoring cellular dye accumulation. This combined fluorescence transport assay was proven to be particularly useful in inhomogeneous cultures, such as transiently transfected cells [24].

In the present work, we employed the GFP-tagged ABCG2 in confocal microscopy studies to determine the kinetics of drug distribution in the plasma membrane and other cellular compartments using the fluorescent anti-cancer agent, mitoxantrone. To investigate whether ABCG2 acts as a classical pump or extrudes its transported substrate directly from the plasma membrane, we generated kinetic models describing the transport processes according to both the classical pump model and the alternative models, and compared the characteristic features of these models with our experimental observations. We found full agreement between experimental data and the models, which indicates substrate recognition by the pump within the plasma membrane.

2. Materials and methods

2.1. Fluorescent drug uptake studies

Cell culturing and expression of GFP-tagged ABCG2 variants in HEK-293 cells was performed as described in [24]. Briefly, the cells were maintained in D-MEM containing 10 % FCS, seeded onto eight-well Lab-Tek II Chambered Coverglass (Thermo Scientific Nunc) at 5×10^4 per well cell density. 24 h after seeding the cells were transfected with GFP-ABCG2 plasmid using the FuGENE® 6 (Roche) in accordance with the manufacturer's instruction. The medium was changed 24 h after transfection. Fluorescent drug transport studies were carried out usually 48 h after transfection, but when cells with various GFP-G2 expression levels were examined, the cultures were studied 24 h after transfection.

To study drug uptake kinetics, the transfected cultures were subjected to 5 μM mitoxantrone (MX) (Sigma-Aldrich) or 2 μm pheophorbide A (Pheo) (Frontier Scientific) in serum free culturing medium (pH 7.4) at room temperature. To block the dye extrusion activity of the transporter, 1 μM Ko143 (gift of Dr. G.J. Kooman) was used approximately 5 min after the addition of the drug. The green (505–525 nm) and far red (> 650 nm) fluorescence were monitored by an Olympus FV500-IX confocal laser scanning microscope using a PLAPO 60× (1.4) oil immersion objective (Olympus) at 488 and 633 nm excitations, respectively. For acquisition and image analysis FluoView (Olympus) software was used.

For efflux studies, transfected cells were incubated with 5 μM MX in the presence of 1 μm Ko143 for 15 min, and washed twice with medium prior to the experiment. Thereafter the fluorescence was monitored as described for the drug uptake experiments.

2.2. Analysis of cellular drug uptake

For kinetic analysis, the cells were classified into two groups (non-transfected and transfected cells) on the basis of green fluorescence. To determine the kinetics of intracellular drug accumulation, the mean far red fluorescence was monitored in various regions of interest (ROIs) positioned in the cell interior apart from the nuclear region. The drug extrusion activity of ABCG2 was expressed by the activity factor calculated from the steady state uptake rates before (F_o) and after (F_i) Ko143 addition by using the formula $(F_i-F_o)/F_i$ as described previously [25]. To correlate activity factor with protein expression at a single cell level, the mean GFP fluorescence was determined in the plasma membrane of the individual cells by placing ROIs over their cell membrane, and the activity factors were plotted against the corresponding GFP fluorescence values.

To study the kinetics of MX accumulation within the plasma membrane, the mean far red fluorescence was monitored in ROIs positioned at the plasma membrane of the cells (c_m). The exact location of the plasma membrane was determined on the basis of GFP fluorescence. Whenever the plasma membrane changed position, the ROI was moved accordingly. The proper tracking of the plasma membrane was verified by the steady green fluorescence values over time (see Fig. 3G). In parallel with monitoring GFP and MX fluorescence in this ROI, the mean far red fluorescence was followed in another ROI with the exact same shape and size, positioned in the cell interior adjacent to the ROI at the plasma membrane. The GFP fluorescence in the second ROI was not different from the background level. The mean far red fluorescence in this ROI was designated as internal or submembrane MX fluorescence (c_i).

2.3. Transport kinetic models

To describe cellular drug uptake and extrusion, various transport kinetic models have been generated. In the first set of models the membrane leaflets are not distinguished, the plasma membrane is considered as a “black box.” In these models the drug distribution has been analyzed in three compartments, i.e., the extracellular space, the plasma membrane, and the intracellular submembrane region (see Fig. 4). Model 0 represents the non-transfected (control) cells, in which no ABCG2 is expressed. Model A corresponds to the ”classical pump” mechanism, in which the transported substrate is expelled from cell interior, whereas model B describes a situation, where the substrate is recognized within the plasma membrane and exported from this compartment. The latter model includes both the “hydrophobic vacuum cleaner” and “floppase” models. To make our models manageable, some reasonable assumptions have been introduced. (i) All transport steps, including ABCG2-mediated transport, are taken as first order kinetic reactions, assuming that the transport capacity of ABCG2 is much larger than the actual transport rate under the given conditions ($c<K_m$). (ii) We have considered the external drug concentration as a constant parameter, based on the fact that the external volume is orders of magnitude larger than the cell membrane volume. Thus, in these three-compartment models there are only two variables: the drug concentration in the membrane (c_m) and in the submembrane region (c_i). The differential equations for the three above mentioned models are as follows.

model 0:

$$\frac{dc_m}{dt} = \frac{1}{V_m}(k_1 c_e - k_2 c_m - k_{-1} c_m + k_{-2} c_i) \quad (1)$$

$$\frac{dc_i}{dt} = \frac{1}{V_i}(k_2 c_m - k_{-2} c_i) \quad (2)$$

model A:

$$\frac{dc_m}{dt} = \frac{1}{V_m}(k_1 c_e - k_2 c_m - k_{-1} c_m + k_{-2} c_i) \quad (3)$$

$$\frac{dc_i}{dt} = \frac{1}{V_i}(k_2 c_m - k_{-2} c_i - k_3 c_i) \quad (4)$$

model B:

$$\frac{dc_m}{dt} = \frac{1}{V_m}(k_1 c_e - k_2 c_m - k_{-1} c_m - k_3 c_m + k_{-2} c_i) \quad (5)$$

$$\frac{dc_i}{dt} = \frac{1}{V_i}(k_2 c_m - k_{-2} c_i) \quad (6)$$

where the designations are as follows: c—concentration, k—rate constant, V—volume; indexes: e—external, m—membrane, i—intracellular (submembrane).

Although our experimental approach is not suitable for distinguishing the individual membrane leaflets, to attempt to discriminate between the "hydrophobic vacuum cleaner" and the "floppase" models, we have generated another set of transport kinetic models, which comprise four compartments (see Fig. 6). In these models, the plasma membrane is divided into two separate compartments, and three variables are considered: the drug concentration in the outer leaflet ($c_{m,e}$), in the inner leaflet ($c_{m,i}$), and in the submembrane region (c_i). There are additional assumptions in these models: (i) the volumes of the inner and outer leaflets are taken as equal; (ii) the rate constants for the passive translocation from the outer leaflet to the inner leaflet ("flip") and for the reverse process ("flop") are considered as an identical parameter (k_m). The differential equations for the four-compartment models are as follows

model 0:

$$\frac{dc_{me}}{dt} = \frac{1}{V_{me}}(k_1 c_e - k_m c_{me} - k_{-1} c_{me} + k_m c_{mi}) \quad (7)$$

$$\frac{dc_{mi}}{dt} = \frac{1}{V_{mi}}(k_m c_{me} - k_m c_{mi} - k_2 c_{mi} + k_{-2} c_i) \quad (8)$$

$$\frac{dc_i}{dt} = \frac{1}{V_i}(k_2 c_{mi} - k_{-2} c_i) \quad (9)$$

In model A, the differential equations are the same as in model 0, with the exception of Eq. (9), which has been modified as follows:

$$\frac{dc_i}{dt} = \frac{1}{V_i}(k_2 c_{mi} - k_{-2} c_i - k_3 c_i) \quad (10)$$

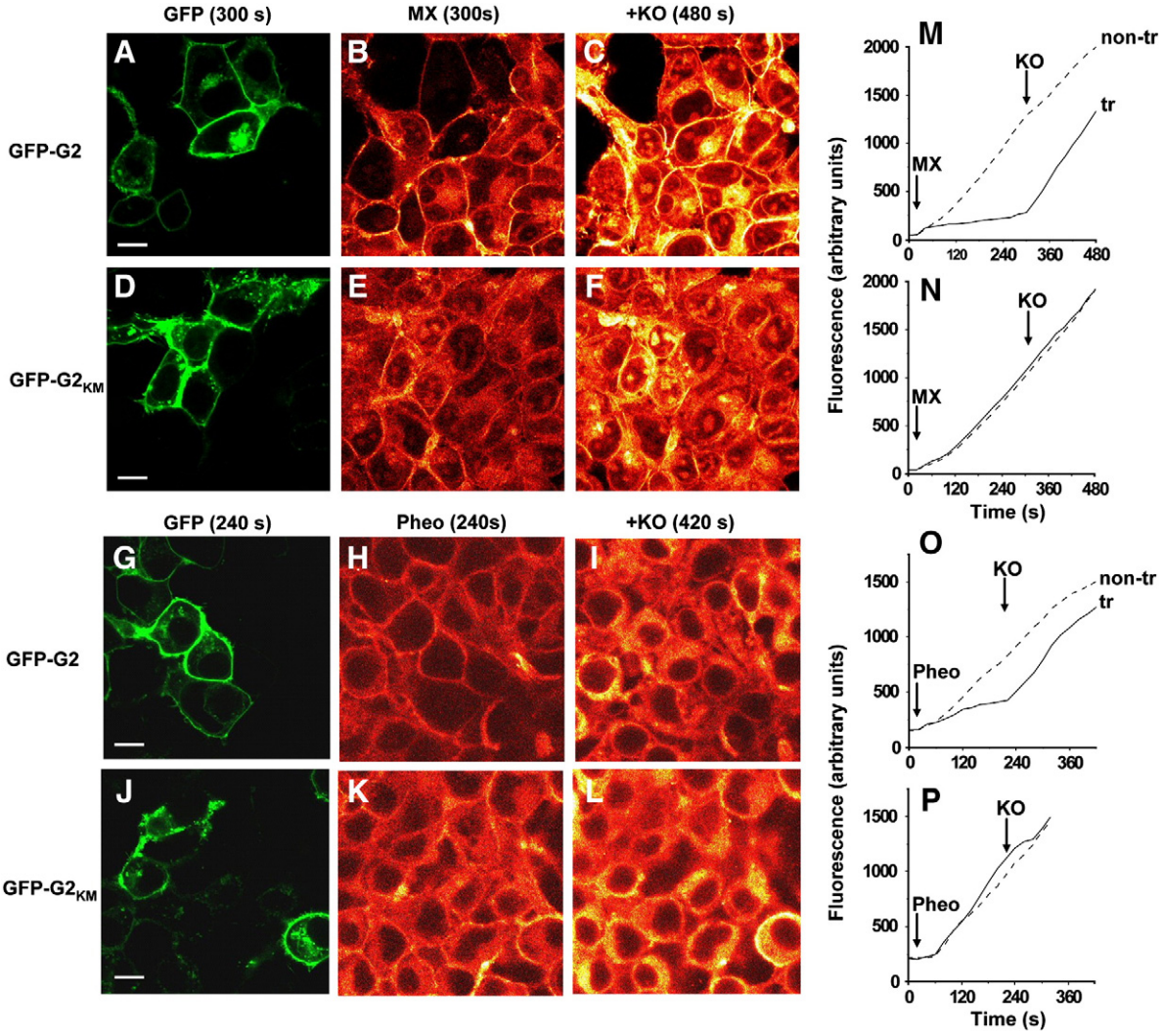

Fig. 1. GFP-tagged ABCG2 prevents cells from intracellular accumulation of fluorescent drugs. HEK-293 cells transfected with GFP-G2 or its inactive mutant variant, GFP-G2$_{KM}$ were subjected to mitoxantrone (MX) (A–F) or pheophorbide A (Pheo) (G–L). Confocal images of GFP fluorescence (A, D, G, J) identify transfected cells, whereas far red fluorescence (pseudo-colored) images depict cellular accumulation of the drugs before (B, E, H, K) and 3 min after the addition of Ko143 (KO), a specific inhibitor of ABCG2 (C, F, I, L). Bars represent 10 μm. The elapsed times are shown in brackets above the images. Time course of drug uptake in cells transfected with GFP-G2 (M, O) or GFP-G2$_{KM}$ (N, P) were also determined and shown by solid lines (tr). Non-transfected cells are represented by dashed lines (non-tr).

In model B, both Eqs. (7) and (8) are altered, but Eq. (9) remains the same as it is in model 0:

$$\frac{dc_{me}}{dt} = \frac{1}{V_{me}}(k_1 c_e - k_m c_{me} - k_{-1} c_{me} - k_3 c_{me} + k_m c_{mi}) \quad (11)$$

$$\frac{dc_{mi}}{dt} = \frac{1}{V_{mi}}(k_m c_{me} - k_m c_{mi} - k_2 c_{mi} - k_3 c_{mi} + k_{-2} c_i) \quad (12)$$

Similarly, in model C, Eq. (9) remains the same, but Eqs. (7) and (8) are modified as follows:

$$\frac{dc_{me}}{dt} = \frac{1}{V_{me}}(k_1 c_e - k_m c_{me} - k_{-1} c_{me} + k_m c_{mi} + k_3 c_{mi}) \quad (13)$$

$$\frac{dc_{mi}}{dt} = \frac{1}{V_{mi}}(k_m c_{me} - k_m c_{mi} - k_2 c_{mi} - k_3 c_{mi} + k_{-2} c_i) \quad (14)$$

For numerical analysis of the kinetic models, first the kinetic parameters of passive drug uptake were determined in both the three-compartment or the four-compartment models. Kinetic curves, based on model 0, were fitted to the pairs of experimental time courses of c_m and c_i values measured in non-transfected (control) cells using the least squares method. For fitting the four-compartment model to the experimental values, c_m was considered as the mean of $c_{m,e}$ and $c_{m,i}$. Once the parameters of passive drug uptake had been determined, predicted kinetic curves based on either model A, model B, or model C were fitted to the pair of experimental time courses of c_m and c_i values of GFP-G2-expressing cells, with k_3 as a single free parameter.

3. Results

3.1. Cellular drug uptake in GFP-G2-transfected cells

In our previous work, the applicability of GFP-G2 in fluorescence transport assay system was demonstrated by using Hoechst 33342, which becomes fluorescent after interaction with cellular DNA [24]. To study the transport mechanism of the ABCG2 multidrug transporter, we chose such known ABCG2 substrates for the transport assay, which gain fluorescence in the lipid environment. The uptake of mitoxantrone (MX) and pheophorbide A (Pheo) were measured in GFP-G2-expressing HEK-293 cells by confocal microscopy, 48 h after transfection (Fig. 1). Transfected and non-transfected cells were identified on the basis of GFP fluorescence, whereas cellular drug uptake was monitored by far red fluorescence. As documented in Fig. 1B, intracellular accumulation of MX was completely prevented in GFP-G2-expressing cells, while rapid drug uptake was observed in non-transfected cells. The addition of Ko143, a specific inhibitor of ABCG2 [26], resulted in a fast accumulation of MX even in the GFP-G2-transfectants without affecting drug uptake in the non-transfected cells (Fig. 1C), demonstrating that the protection from drug uptake is due to the transport activity of GFP-G2. The specificity of drug extrusion was further supported by the observation that a catalytic site mutant variant of GFP-G2 (GFP-$G2_{K86M}$) did not prevent MX uptake (Fig. 1D–F). Accordingly, for this construct Ko143 addition had no effect on intracellular drug uptake in either transfected or non-transfected cells. Similar results were obtained when Pheo uptake was measured in GFP-G2- and GFP-$G2_{KM}$-transfected cells (Fig. 1G–L). The kinetic curves of intracellular drug accumulation were also obtained from the image sequences (Fig. 1M–P). Activity factors were calculated from the drug uptake rates before (F_o) and after (F_i) inhibitor addition by the formula $(F_i - F_o)/F_i$ as described previously [25]. In GFP-G2-expressing cells these activity factors were 0.89 and 0.86 for MX and Pheo, respectively, whereas these values were 0 for both dyes in either non-transfected or GFP-$G2_{KM}$-expressing cells.

24 h after transfection, the expression levels vary from cell to cell. When dye uptake kinetics and activity factors were determined in individual cells with different expression levels of GFP-G2 (Fig. 2A–C), a close correlation between the activity factor and plasma membrane GFP-fluorescence was found (Fig. 2D). The characteristics of this relationship are similar to those reported previously for MDR1-expressing cells [25].

3.2. Determination of drug uptake kinetics in the plasma membrane

As mentioned above, in contrast to Hoechst 33342, MX and Pheo become fluorescent in non-polar environment [27,28]. We observed that some accumulation of MX also takes place in the plasma membrane of GFP-G2-expressing cells (Fig. 3D–E), whereas drug uptake into the internal membranes can be seen only after the inhibition of the transporter (Fig. 3F). Tracking the position of the plasma membrane in the GFP image allows determining the kinetics of MX accumulation separately in the plasma membrane and in the submembrane regions (Fig. 3G). Drug concentration in the plasma membrane rapidly saturates in GFP-G2-expressing cells, whereas in non-transfected cells it shows a continuous increase within the studied time frame (Fig. 3H). Uptake into the internal membranes monotonically increased in both cell types, although the uptake rate was much higher in control cells than in transfectants. GFP-$G2_{KM}$-expressing cells exhibited drug accumulation kinetics similar to that seen in control cells (Fig. 3I), demonstrating that the observed

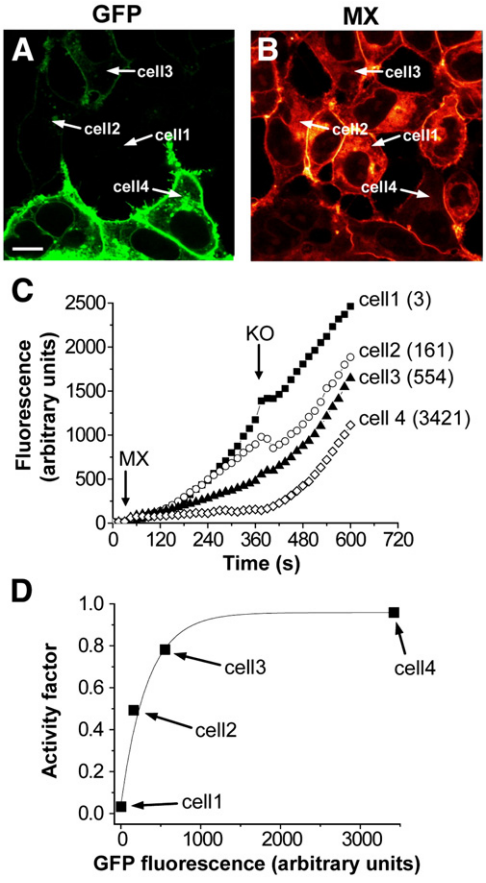

Fig. 2. Analysis of mitoxantrone uptake in cells expressing different levels of GFP-G2. Confocal images of green (A) and far red fluorescence (B) are shown 5 min after MX addition. Bar represents 10 μm. (C) Kinetic curves of intracellular accumulation of MX in four selected cells indicated by arrows in the images. The numbers represent the mean fluorescence intensities of GFP in the plasma membrane. (D) Correlation of the expression level with the ABCG2-mediated drug extrusion activity factor calculated as described previously [25].

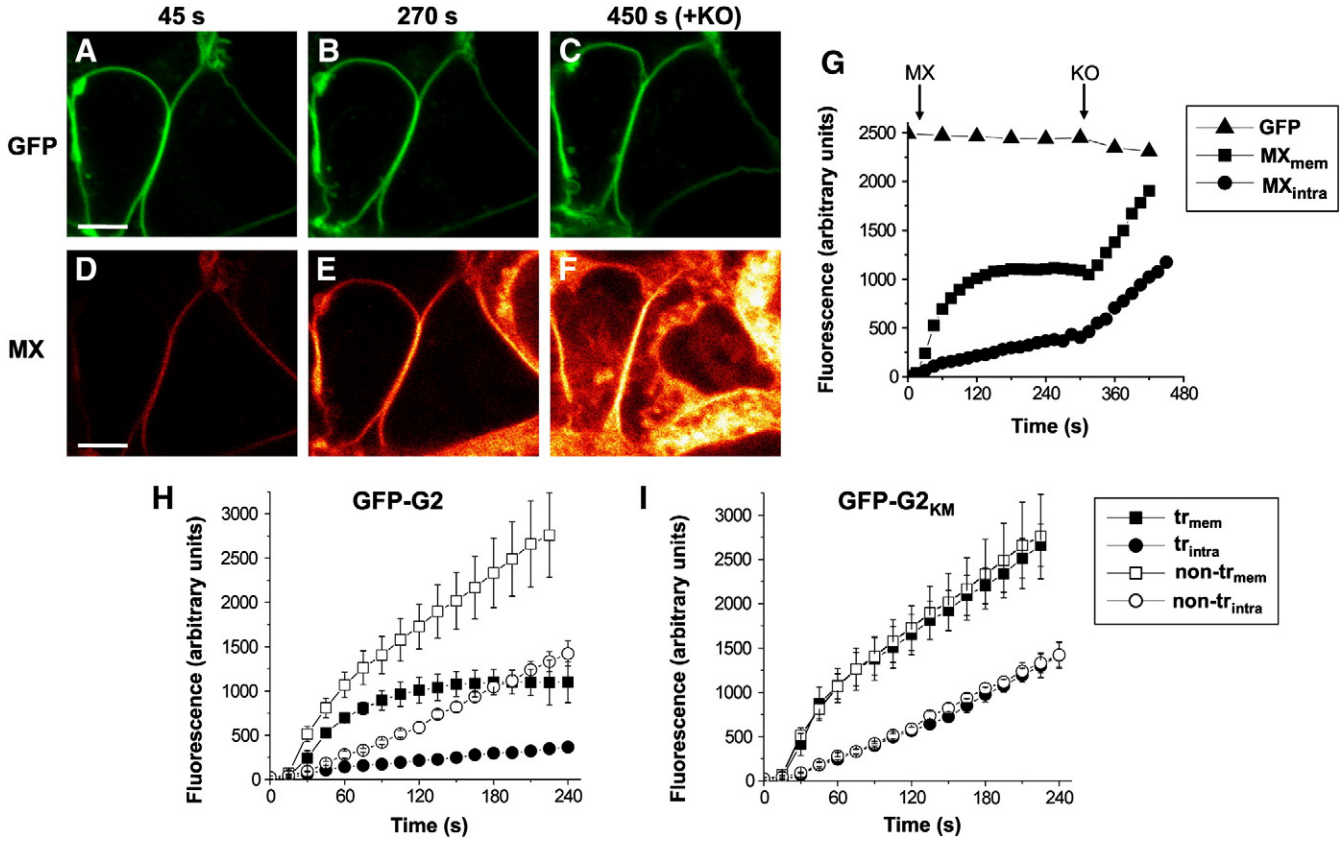

Fig. 3. Quantitative determination of mitoxantrone accumulation in the plasma membrane. (A–F) Image sequence of a representative mitoxantrone uptake experiment performed with GFP-G2-transfected HEK-293 cells (for details see the legend of Fig. 1). (A–C) GFP fluorescence; (D–F) far red fluorescence; numbers on the top indicate the elapsed time in seconds; bars represent 5 μm. The ABCG2 inhibitor KO was added at around 300 s. (G) Kinetic analysis of mitoxantrone uptake experiment shown in Panels A–F. The plasma membrane was tracked by a region of interest (ROI) on the basis of GFP fluorescence (GFP, triangles). MX accumulation into the plasma membrane was determined by using the same ROI in the far red fluorescence images (MX_{mem}, squares) while the submembrane dye concentration was measured by another ROI situated next to the first one, inside the cell (MX_{intra}, circles). (H, I) Comparison of mitoxantrone uptake into the plasma membrane (mem, squares) and the submembrane region (intra, circles) of GFP-G2- and GFP-$G2_{KM}$-transfected cells (tr, filled symbols) to that of non-transfected (non-tr, empty symbols) cells. Values are means ± S.E.M. of at least four independent experiments.

saturation of the drug level in the plasma membrane of GFP-G2-expressing cells is due to the activity of the transporter. This notion is further supported by the observation that addition of Ko143 to GFP-G2-expressing cells resulted in rapid and continuous elevation in the plasma membrane drug concentration (Fig. 3G).

3.3. Transport kinetic models of cellular drug uptake

To evaluate the kinetics of drug accumulation in the plasma membrane and the internal membranes, we generated various transport kinetic models, which describe cellular drug uptake and extrusion. Since the experimentally measured parameter is the integral average of MX fluorescence across the entire plasma membrane, as a first approach a three-compartment model was used, in which the plasma membrane was considered as a "black box", the membrane leaflets are not distinguished. Using the three-compartment scheme, three different models were generated: model 0 describes the drug movement in the non-transfected (control) cells, whereas model A and model B illustrate the situation with the GFP-G2-transfected cells. Model A corresponds to the "classical pump" mechanism, in which the transported substrate is expelled from cell interior. In model B the substrate is recognized within the plasma membrane, thus, this model combines the "hydrophobic vacuum cleaner" and the "floppase" models (see Fig. 4A–C).

These three-compartment models implicitly suggest that the passive transition rate between the membrane leaflets is not a rate limiting step, thus, it is larger than the diffusion rates to any other compartments. This assumption is reasonable, considering the chemical properties of mitoxantrone at pH 7.4, the pH value of the experiments. This drug is a very weak base, has four amines with two different dissociation constants (pKa 5.99 and 8.13 in pairs), thus, it is slightly positively charged at physiological pH. Mitoxantrone is a hydrophobic molecule, sparingly soluble in water even in its hydrochloride form [29]. It is more soluble in octanol, but its solubility is extremely good in lipids as demonstrated in Ref. [30]. The lipid/water partitioning coefficient for mitoxantrone was found to be 230,000. Taking together these characteristics of mitoxantrone, it is reasonable to assume that it crosses the plasma membrane at a high rate. This notion is in accordance with our experimental observation that MX rapidly accumulates within the non-transfected cells.

To describe our models mathematically, we employed some other assumptions. The transport activity of ABCG2 was described with a first order kinetics, on the basis of the fact that the transport capacity substantially exceeds the particular transport rate under the given conditions ($c<K_m$). Similarly, we assumed that the external drug concentration (c_e) is constant. Although the lipid/water partitioning coefficient for mitoxantrone is relatively high (230,000) [30] as mentioned earlier, the several orders of magnitude difference between the volume of the external space and the cell membranes along with the short time frame of the study makes this assumption reasonable. The differential equations for the three different models are given in Section 2.3 (Eqs. (1)–(6)).

For closed-form solution of the differential equations, we also assumed that the rate constants for spontaneous drug equilibration

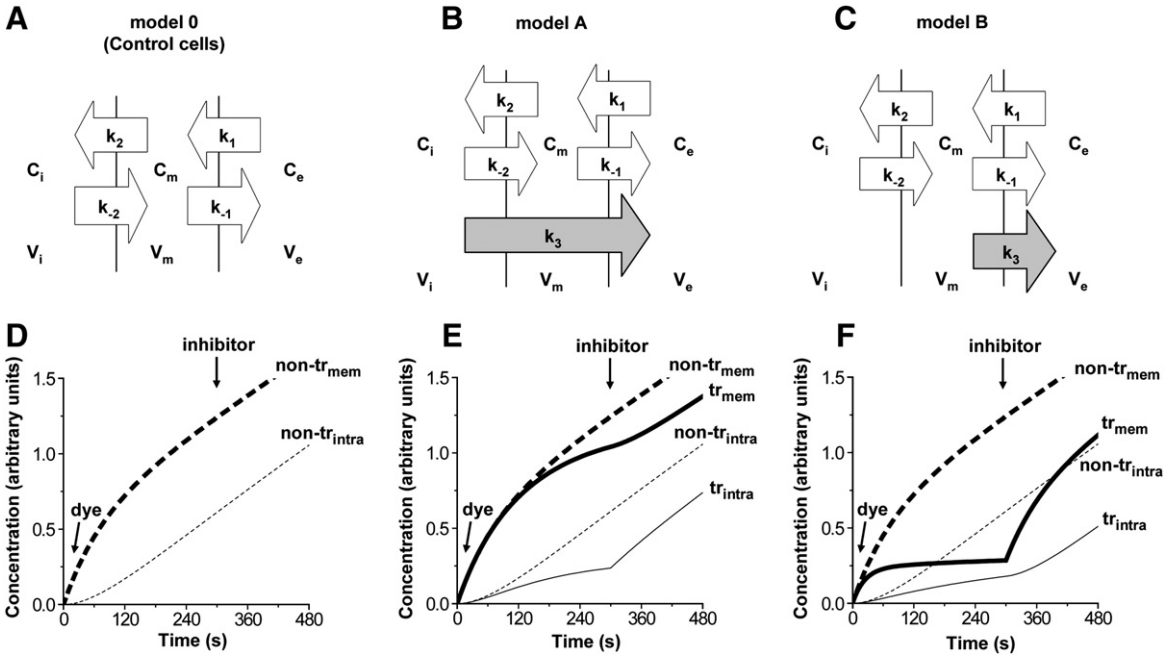

Fig. 4. Kinetic models describing drug uptake and extrusion by a multidrug transporter. (A) Drug uptake into non-transfected, control cells (model 0); (B) Classical pump mechanism, where the substrate transported from the cytosole (model A); (C) an alternative model, in which the transporter expels its substrate directly from the membrane (model B). The variables are as follows: *c*—concentration, *k*—rate constant, *V*—volume; indexes: *e*—external, *m*—membrane, *i*—intracellular. The differential equations for these models are given in Section 2.3 (Eqs. (1)–(6)). (D–E) Closed-form solutions of the kinetic models. Dashed lines: non-transfected cells (non-tr), solid lines: transfected cells (tr); thick lines: plasma membrane concentrations (mem); thin lines: intracellular concentrations (intra). At the time point 300 s k_3 is made equal to 0, mimicking the addition of the inhibitor.

between the plasma membrane and intracellular compartments are identical both ways ($k_2 = k_{-2}$), based on the consideration that the measured intracellular drug concentration (c_i) reflects the mitoxantrone level in internal membranes, thus, in another lipid environment.

Parametric solution of the differential equations elucidated various qualitative distinguishing features of the different models. (i) In model A, the plasma membrane concentration of the drug (c_m) in transfectants differs only slightly from the c_m value in control cells, whereas in model B, c_m rapidly saturates at a greatly reduced level (Fig. 4E–F). (ii) It is also easy to show that the equilibrium values for c_m and c_i are different in model A, whereas they approach the same equilibrium value in model B. For mathematical verification see Statement 1 in the Appendix. iii) Upon addition of an inhibitor to the system, i.e., when k_3 is suddenly made 0, model A predicts a prompt increase in c_i, followed with a delay by an elevation in c_m. In contrast, in model B c_m elevates first and c_i lags behind. In other words, if an inhibitor is added when the system has already reached equilibrium, then model A predicts a positive value for the initial slope of c_i and a zero value for that of c_m, whereas for model B the initial slope of c_m is positive and that of c_i is zero. The detailed mathematical demonstrations of this statement (Statement 2) can be found in the Appendix.

3.4. Comparison of experimental data with the kinetic models

The experimental time courses shown in Fig. 5A are congruent with the features of model B, i.e. (i) c_m in transfected cells rapidly saturates, (ii) c_m and c_i seem to tend towards the same equilibrium (see below), and (iii) c_m promptly increases after the addition of the inhibitor (Fig. 5A). To study the equilibrium of c_m and c_i values further, we performed an extended uptake experiment without adding inhibitor to the cells. This experiment also confirmed the validity of model B, since c_m and c_i approach the same equilibrium value (Fig. 5B).

To determine the kinetic parameters of passive drug uptake (k_1, k_{-1}, k_2, k_{-2}) in our system, we fitted kinetic curves based on model 0 to the pairs of experimental c_m and c_i time courses of non-transfected cells, using the least squares method (Fig. 5A, dashed lines, RMSE = 75.3). Interestingly, the fitting returned k_2 equal to k_{-2}, as was previously assumed based on theoretical considerations for obtaining closed-form solutions (see above). Using these parameters we then fitted kinetic curves, based on either model A or model B, to the pairs of experimental c_m and c_i time courses of transfected cells, with k_3 as the single free parameter. While the fit was unacceptable when model A was used (RMSE = 655.7, not shown), we obtained a reasonable fit using model B (Fig. 5A, solid lines, RMSE = 158.7). It is noteworthy that the obtained value for k_3 was 10^8-fold larger than k_2 or k_{-2} when model A was fitted, whereas this ratio proved to be only 35 when model B was used. In other words, overcoming drug influx would require extremely high transport rates if the drug were extruded from the cytoplasm, whereas a reasonable transport rate can efficiently compensate for the influx if the drug is expelled directly from the membrane.

3.5. Kinetics of drug efflux and equilibrium drug concentrations

In addition to drug uptake, we also studied efflux of mitoxantrone from preloaded cells. It is easily conceivable that the drug concentration should decrease first in the intracellular compartment, and its plasma membrane concentration should fall with a delay, if the drug were extruded from the cell's interior (model A). However, the efflux experiment shown in Fig. 5C demonstrates the reverse situation, i.e. the drug concentration drops first in the membrane followed with a delay by a decrease in c_i,—a scenario which is in accordance with model B.

Finally, we determined the equilibrium concentrations of mitoxantrone in the plasma membrane ($c_{m,eq}$) in cells expressing different amounts of GFP-G2 as demonstrated in Fig. 5D–E. The inverses of these values were correlated with GFP-fluorescence, which is

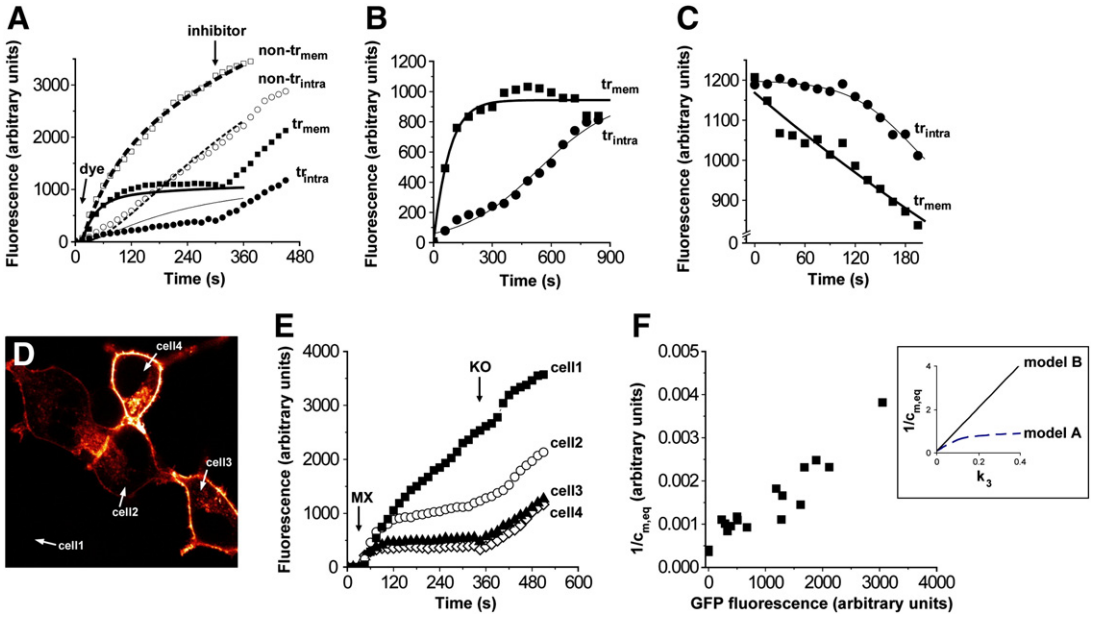

Fig. 5. Experimental evaluations of model predictions on cellular drug accumulation. (A) Experimental values of mitoxantrone uptake into the plasma membrane (mem, squares) and the submembrane region (intra, circles) of GFP-G2-transfected (tr, filled symbols) and non-transfected cells (non-tr, empty symbols). Values are means of at least four independent experiments, error bars are not shown to avoid confusion. Dashed lines represent fitted kinetic curves based on model 0 to the pairs of experimental c_m and c_i time courses of non-transfected cells. Similar fitted curves based on model B to the experimental values of GFP-G2-expressing cells are shown by solid lines. Thick lines: plasma membrane concentrations; thin lines: intracellular concentrations. (B) Determination of equilibrium values of mitoxantrone uptake in GFP-G2-transfected cells. Kinetics of drug uptake into the plasma membrane (tr_{mem}, squares) and the intracellular space (tr_{intra}, circles) are shown in a representative extended experiment. Symbols: squares—plasma membrane; circles—intracellular concentrations. (C) Time course of drug efflux from cells preloaded with mitoxantrone. Symbols are the same as in Panel B. (D) Representative experiment demonstrating mitoxantrone uptake in cells expressing various levels of GFP-G2. (E) Kinetics of mitoxantrone uptake into the plasma membrane of the cells shown in Panel D. (F) Correlation of the inverses of the equilibrium concentrations of mitoxantrone in the plasma membrane ($1/c_{m,eq}$) in different GFP-G2-expressing cells with the corresponding GFP fluorescence. Each symbol represents a value pair ($1/c_{m,eq}$–GFP fluorescence) for an individual cell; data derived from four independent experiments. Inset shows model predictions: dependency of $1/c_{m,eq}$ value on k_3 is indicated for both model A and B (for detailed mathematical explanation see Statement 3 in the Appendix).

proportional to the expression level of the transporter, i.e., to the rate constant k_3. Model A suggests a saturating curve when $1/c_{m,eq}$ is plotted against k_3, whereas model B predicts a linear relationship (inset in Fig. 5F) (for explanation see Statement 3 in the Appendix). The experimental values exhibit a linear correlation between $1/c_{m,eq}$ and GFP fluorescence, providing further support for the validity of model B (Fig. 5F).

3.6. Four-compartment kinetic models

As discussed above, the three-compartment models imply that the passive transition across the membrane is not a rate limiting step. Although this assumption seemed reasonable on the basis of the chemical properties of mitoxantrone, we considered the possibility that the membrane translocation rate is comparable with the rates of the other steps, and generated another set of models, in which the membrane leaflets were considered as separate compartments (Fig. 6A–D). Similar to the designation used earlier, model 0 describes the drug movement in the control cells; model A illustrates the "classical pump" mechanism. Nevertheless, this four-compartment model scheme allowed us to distinguish between the "hydrophobic vacuum cleaner" (model B) and the "floppase" mechanisms (model C). To keep the number of parameters at a reasonable level, equal volumes for the inner and outer leaflets were assumed, as well as the rate constants for passive inward and outward translocation in the membrane were described with a single parameter (k_m). The differential equations for the four-compartment models are given in Section 2.3 (Eqs. (7)–(14)).

Due to resolution limits, our experimental approach does not allow discriminating between the individual membrane leaflets. Therefore, only two experimental parameters were measured: the mean MX fluorescence across the entire plasma membrane (c_m) and in the submembrane region (c_i). When fitting the four-compartment models, this measured c_m value was compared with the arithmetic mean of the predicted $c_{m,i}$ and $c_{m,e}$ values. Similar to the method used for the three-compartment models, first the kinetic parameters of passive drug uptake (k_1, k_{-1}, k_2, k_{-2}, k_m) were determined by fitting the four-compartment model 0 to the pair of the kinetic curves (c_m and c_i) measured in the non-transfected cells (Fig. 6A). This resulted in a reasonable fit (RMSE = 75.7, Fig. 6E), and again returned k_2 equal to k_{-2}. In addition, the membrane translocation rate (k_m) was obtained to be 16-fold larger than k_{-1} and 60-fold larger than k_2 or k_{-2}, supporting our previous assumption that the passive transition across the membrane is not a rate limiting step.

Using the parameters obtained for the control cells and model 0, the experimental c_m and c_i time courses of GFP-G2-expressing cells were fitted either with model A, model B, or model C, with k_3 as a single free parameter (Fig. 6F–H). Similar to that seen in the case of the three-compartment models, the fit was unacceptable when model A was used (Fig. 6F, RMSE = 652.1). A substantially better fit was obtained on the basis of model B (Fig. 6G, RMSE = 155.2), nevertheless, the best fit was obtained when model C, corresponding to the "floppase" mechanism, was used (Fig. 6H, RMSE = 38.1).

In addition to separately fitting the time courses of control and GFP-G2-expressing cells, we also performed ensemble fits of all 8 free parameters to all four kinetic curves using either model A, model B, or model C. A reasonable fit was obtained only when model C was used (RMSE = 63.4), returning the same kinetic parameters obtained by the separate fitting approach. In contrast, 8-parametric fitting with models A and B resulted in unacceptable fits and meaningless parameters, e.g., negative rate constants.

In the four-compartment models, we assumed that the passive "flip" and "flop" rate constants are identical (k_m). To examine whether this assumption is acceptable, we also analyzed a model in which

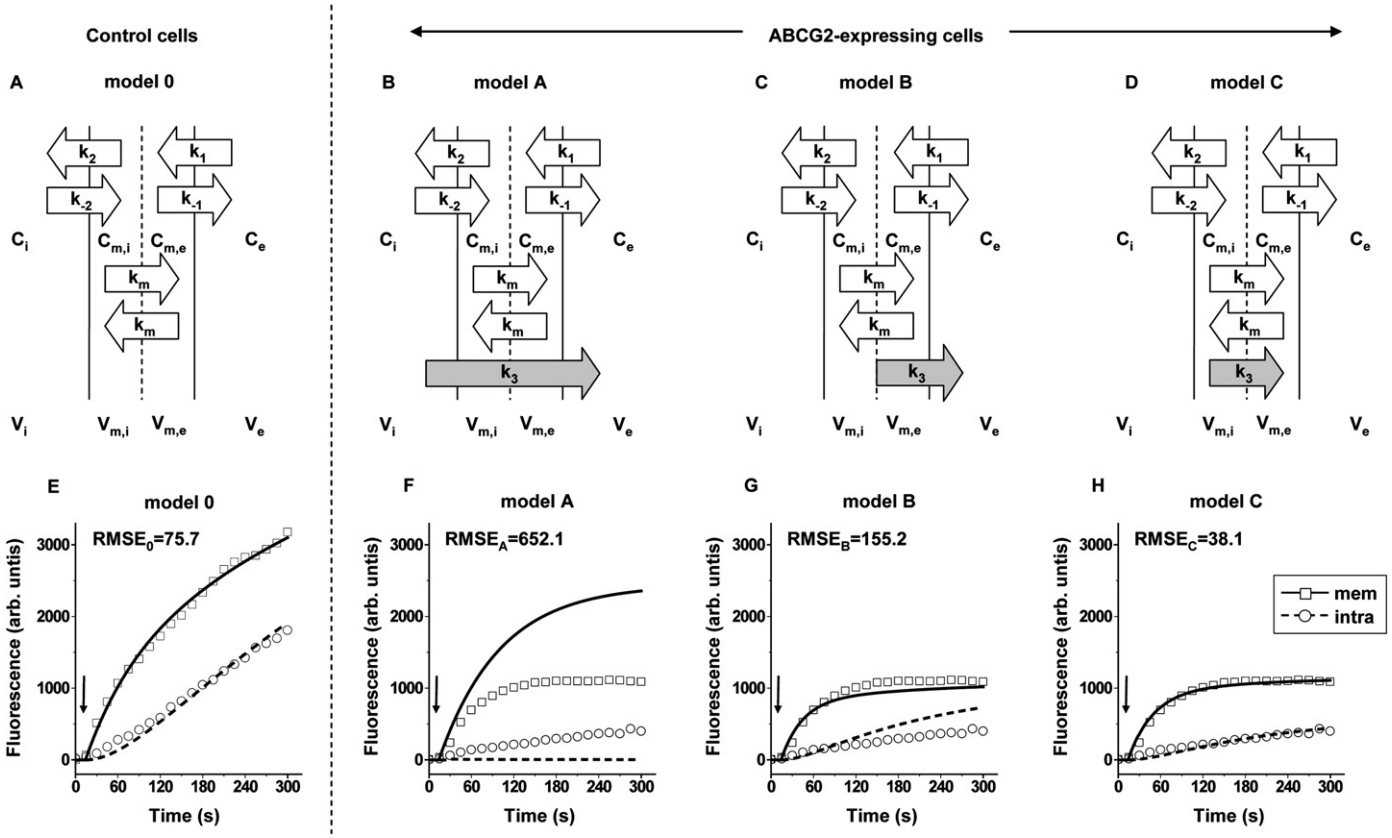

Fig. 6. Numerical analysis of kinetic models comprising four compartments. In these model schemes the membrane leaflets are considered as separate compartments. (A) Model 0 describes drug distribution in non-transfected (control cells); (B–D) drug movement in GFP-G2-espressing cells is shown in accordance with different transport models: the "classical pump" (model A), the "hydrophobic vacuum cleaner" (model B) and the "floppase" (model C) mechanisms. Designations are similar used in Fig. 4: *c*—concentration, *k*—rate constant, *V*—volume; indexes: *e*—external, *m*—membrane, *i*—intracellular; *m,i*—inner membrane leaflet; *m,e*—outer membrane leaflet. The differential equations for these models are given in Section 2.3 (Eqs. (7)–(14)). (E–H) The four-compartment models were fitted to the experimental time courses of mitoxantrone uptake into the plasma membrane (mem, squares) and the submembrane region (intra, circles). The solid lines represent the fitted kinetic curves to membrane MX fluorescence time course, whereas the dashed lines indicate the intracellular (submembrane) values. The fittings were based on the corresponding models shown above. The experimental values of control cells were fitted with 7 free parameter using model 0. These parameters were then used for fitting the other models to the time courses of GFP-G2-expressing cells, with k_3 as a single free parameter. The quality of the fits is represented by the root mean square error (RMSE) values. Arrows mark the addition of the drug.

these rate constants were independent variables ($k_{m,i}$ and $k_{m,e}$). Interestingly, the fit using this model scheme returned a $k_{m,i}/k_{m,e}$ ratio close to 1, verifying the applicability of our original assumption. Finally, we also examined a modified model B. In our "hydrophobic vacuum cleaner" model, drug extrusion was allowed from both leaflets (see Fig. 6C). We analyzed a model scheme in which the transported substrate is exported exclusively from the inner leaflet. This modification of model B had little effect on the fit (data not shown, RMSE = 152.1).

Taken together, the four compartment models provide further support to the notion that the drug is transported by ABCG2 from the plasma membrane, rather than from the cell interior. Moreover, this approach prefers the "floppase" mechanisms over the "hydrophobic vacuum cleaner" model.

4. Discussion

To investigate the substrate-transporter interaction, we employed the fully functional fluorescently labeled multidrug transporter, GFP-tagged ABCG2 [24] in an on-line confocal microscopic assay system. The GFP-tag allowed us to identify the ABCG2-expressing cells and to track down the position of the plasma membrane in living cells. We studied the cellular uptake of well-known fluorescent substrates of ABCG2, mitoxantrone and pheophorbide A. The peculiarity of this experimental setup is that these compounds become fluorescent in the lipid environment, which feature made possible to determine the drug concentration in the plasma membrane. We performed a detailed kinetic analysis of drug uptake and efflux, and found that (i) the plasma membrane drug concentration (c_m) rapidly saturates in the AGCG2-expressing cells as compared to control cells; (ii) the plasma membrane and intracellular drug concentrations approach to the same equilibrium value ($c_{m,eq} = c_{i,eq}$); (iii) the drug concentration increases first in the plasma membrane, when ABCG2 is inhibited; (iv) the drug concentration drops first in the plasma membrane in the efflux experiment; (v) there is a linear relationship between $1/c_{m,eq}$ values and GFP fluorescence. Numerical analysis of both the three-compartment and four-compartment models resulted in reasonable fits only when transport from plasma membrane was assumed (model B and model C). Acceptable fit was never obtained with model A.

Taken together, all observed characteristics of mitoxantrone uptake and efflux experiments in concert disprove model A, which corresponds to the "classical pump" mechanism. Classical pumps translocate the transported substrate from the cytosole to the external space through a pore. In contrast, in the "hydrophobic vacuum cleaner" model, drugs partition into the membrane and are expelled by the transporter directly from the lipid bilayer. In the "floppase model", drugs are translocated by the transporter from the cytoplasmic leaflet to the external leaflet of the lipid bilayer. This redistribution of the drug along with the portioning between the membrane leaflets and the aqueous phases results in a net flux of the drug. Both the hydrophobic vacuum cleaner and floppase models suggest

substrate recognition within the lipid bilayer. Our three-compartment model B, considering the membrane as a "black box", also based on substrate recognition within the membrane, and combines these two mechanisms. The four compartment model scheme, however, where the membrane leaflets are distinguished, may allow discriminating between the "hydrophobic vacuum cleaner" and the "floppase" models. Numerical analysis of these models showed a slight preference for the "floppase" mechanism, although we do not feel confident to exclude the "hydrophobic vacuum cleaner" model on the basis of our results. Nevertheless, all approaches clearly invalidated the "classical pump" mechanism.

As mentioned earlier, c_i is in fact not the cytoplasmic concentration of MX, but reflects the drug level in the internal membranes adjacent to the plasma membrane. Thus, disapproval of model A at first excludes only the mechanism that the drug is expelled directly from the internal membrane. Nevertheless, if we assume drug extrusion from an aqueous layer (quasi cytoplasm) located between the plasma membrane and the internal membrane compartments, at least a mixed behavior should be observed, since the drug diffuses equally to both neighboring compartments. It is easy to see, for instance, that there would always be a difference in the equilibrium c_m and c_i values ($c_{m,eq}$, $c_{i,eq}$), or that c_m and c_i would decrease with the same delay in the efflux experiment, or that there would be no linear relationship between $1/c_{m,eq}$ and the expression level, if the changes in the membrane drug concentrations are indirect consequence of drug extrusion from the "cytoplasmic" compartment and redistribution of drug by passive diffusion. Since all the arguments, listed here and above, unambiguously support the validity of model B in the three-compartment model, we can excluded drug extrusion from the aqueous phase.

Some ABC transporters, e.g. MRP1, are known to transport their substrates by multiple transport mechanisms [4]. Thus, it is plausible to raise the question whether ABCG2 might extrude drugs from both the cytoplasm and the plasma membrane. Our observations exclude the possibility of such a mixed transport mechanism, since c_m and c_i approach the same equilibrium (Fig. 5B), and $1/c_{m,eq}$ exhibited clear linear relationship with k_3 (Fig. 5F). However, it should be mentioned that our studies were limited to the transport mechanism of one particular drug, mitoxantrone. It is still possible that other, less hydrophobic substrates of ABCG2 are transported via the classical mechanism. It is especially plausible to assume this for water soluble ABCG2 substrates, such as topotecan, although most ABCG2 substrates, such as flavopiridol, methotrexate, Imatinib mesylate, or pheophorbide A are strongly hydrophobic.

5. Conclusions

Our study clearly indicates that the anti-cancer drug, mitoxantrone is expelled by ABCG2 directly from the plasma membrane, providing unambiguous experimental evidence for the non-canonical way of action of a multidrug protein. In general, this mechanism can explain the extremely broad substrate recognition of the multidrug transporters, which feature is indispensable for fulfilling their special physiological role. In addition, our novel experimental approach, using substrate molecules, which are fluorescent in the lipid environment, combined with transport kinetic analysis, offers a new tool for studying the mechanism of membrane transporters.

Acknowledgements

This work has been supported by research grants from OTKA (K68936, CK80283, T48986), ETT (211-09), NKFP-1A-060/2004, and KMOP-1.1.2-07/1-2008-0003. T. I. Orbán and L. Csanády have been recipients of the János Bolyai Scholarship of the Hungarian Academy of Sciences. We appreciate the technical help of Gyöngyi Bézsenyi. We thank for the valuable advice of Zoltán Noszticiusz.

Appendix

For comparison of the kinetic models with experimental data, various features of the models were used. These features, given as statements, can be mathematically verified as follows.

Statement 1: the equilibrium values for c_m and c_i are different in model A, whereas they approach the same equilibrium value in model B. In equilibrium dc_i/dt is equal to 0, the relation between the equilibrium values of c_m and c_i can be expressed from Eqs. (4) and (6) as follows

model A:

$$c_{m,eq} = \frac{k_{-2} + k_3}{k_2} c_{i,eq} \tag{A.1}$$

model B:

$$c_{m,eq} = \frac{k_{-2}}{k_2} c_{i,eq} \tag{A.2}$$

With the assumption that $k_2 = k_{-2}$ (for explanation see Section 3.3),

model A:

$$c_{m,eq} = \left(1 + \frac{k_3}{k_2}\right) c_{i,eq} \tag{A.3}$$

model B:

$$c_{m,eq} = c_{i,eq} \tag{A.4}$$

Since k_3 and k_2 are positive values, $c_{m,eq}$ is always greater than $c_{i,eq}$ in model A, whereas they are equal in model B.

Statement 2: if an inhibitor is added when the system has already reached equilibrium, then model A predicts a positive value for the initial slope of c_i and a zero value for that of c_m, whereas for model B the initial slope of c_m is positive and that of c_i is zero. To prove this statement Eqs. (3)–(6) were made equal to zero, and the equilibrium values of c_m and c_i were expressed as follows

model A:

$$c_{m,eq} = \frac{k_1(k_{-2} + k_3)}{k_2 k_3 + k_{-1}(k_{-2} + k_3)} c_e \tag{A.5}$$

$$c_{i,eq} = \frac{k_1 k_2}{k_2 k_3 + k_{-1}(k_{-2} + k_3)} c_e \tag{A.6}$$

model B:

$$c_{m,eq} = \frac{k_1}{k_{-1} + k_3} c_e \tag{A.7}$$

$$c_{i,eq} = \frac{k_1 k_2}{k_{-2}(k_{-1} + k_3)} c_e \tag{A.8}$$

Eqs. (A.5) and (A.6) were introduced into Eq. (1) or Eq. (2), mimicking complete inhibition by the inhibitor by model 0

model A:

$$\frac{dc_m}{dt} = 0 \tag{A.9}$$

$$\frac{dc_i}{dt} = \frac{k_3 c_{i,eq}}{V_i} \tag{A.10}$$

The latter is always greater then zero, since k_3, $c_{i,eq}$ and V_i are positive values. Similarly, introducing Eqs. (A.7) and (A.8) into Eq. (1) or Eq. (2) yields

model B:

$$\frac{dc_m}{dt} = \frac{k_3 c_{m,eq}}{V_m} \tag{A.11}$$

$$\frac{dc_i}{dt} = 0 \tag{A.12}$$

The former is always greater then zero, since k_3, $c_{m,eq}$ and V_m are positive values.

Statement 3: model A suggests a saturating curve when $1/c_{m,eq}$ is plotted against k_3, whereas model B predicts a linear relationship. Rearrangement of Eqs. (A.5) and (A.7) yields

model A:

$$\frac{1}{c_{m,eq}} = \frac{k_{-1}}{k_1 c_e} + \frac{1}{k_1 c_e} \cdot \frac{k_2 k_3}{k_{-2} + k_3} \tag{A.13}$$

model B:

$$\frac{1}{c_{m,eq}} = \frac{k_{-1}}{k_1 c_e} + \frac{k_3}{k_1 c_e} \tag{A.14}$$

Since the volume of the external space is several orders of magnitude larger than that of the cells, c_e is considered as constant, thus, Eq. (A.14) shows linear relationship between $1/c_{m,eq}$ and k_3. In contrast, on the basis of Eq. (A.13), $1/c_{m,eq}$ approaches $(k_{-1}+k_2)/(k_1 c_e)$ as k_3 becomes extremely large.

References

[1] M.M. Gottesman, T. Fojo, S.E. Bates, Multidrug resistance in cancer: role of ATP-dependent transporters, Nat. Rev. Cancer 2 (2002) 48–58.
[2] B. Sarkadi, L. Homolya, G. Szakacs, A. Varadi, Human multidrug resistance ABCB and ABCG transporters: participation in a chemoimmunity defense system, Physiol. Rev. 86 (2006) 1179–1236.
[3] R.G. Deeley, C. Westlake, S.P. Cole, Transmembrane transport of endo- and xenobiotics by mammalian ATP-binding cassette multidrug resistance proteins, Physiol. Rev. 86 (2006) 849–899.
[4] E. Bakos, L. Homolya, Portrait of multifaceted transporter, the multidrug resistance-associated protein 1 (MRP1/ABCC1), Pflugers Arch. 453 (2007) 621–641.
[5] G. Szakacs, A. Varadi, C. Ozvegy-Laczka, B. Sarkadi, The role of ABC transporters in drug absorption, distribution, metabolism, excretion and toxicity (ADME-Tox), Drug Discov. Today 13 (2008) 379–393.
[6] P. Borst, J. Jonkers, S. Rottenberg, What makes tumors multidrug resistant? Cell Cycle 6 (2007) 2782–2787.
[7] G. Szakacs, J.K. Paterson, J.A. Ludwig, C. Booth-Genthe, M.M. Gottesman, Targeting multidrug resistance in cancer, Nat. Rev. Drug Discov. 5 (2006) 219–234.
[8] R.W. Robey, O. Polgar, J. Deeken, K.W. To, S.E. Bates, ABCG2: determining its relevance in clinical drug resistance, Cancer Metastasis Rev. 26 (2007) 39–57.
[9] F.J. Sharom, ABC multidrug transporters: structure, function and role in chemoresistance, Pharmacogenomics 9 (2008) 105–127.
[10] O. Polgar, S.E. Bates, ABC transporters in the balance: is there a role in multidrug resistance? Biochem. Soc. Trans. 33 (2005) 241–245.
[11] Y. Raviv, H.B. Pollard, E.P. Bruggemann, I. Pastan, M.M. Gottesman, Photosensitized labeling of a functional multidrug transporter in living drug-resistant tumor cells, J. Biol. Chem. 265 (1990) 3975–3980.
[12] M.M. Gottesman, I. Pastan, Biochemistry of multidrug resistance mediated by the multidrug transporter, Annu. Rev. Biochem. 62 (1993) 385–427.
[13] C.F. Higgins, M.M. Gottesman, Is the multidrug transporter a flippase? Trends Biochem. Sci. 17 (1992) 18–21.
[14] L. Homolya, Z. Hollo, U.A. Germann, I. Pastan, M.M. Gottesman, B. Sarkadi, Fluorescent cellular indicators are extruded by the multidrug resistance protein, J. Biol. Chem. 268 (1993) 21493–21496.
[15] H. Bolhuis, H.W. van Veen, D. Molenaar, B. Poolman, A.J. Driessen, W.N. Konings, Multidrug resistance in *Lactococcus lactis*: evidence for ATP-dependent drug extrusion from the inner leaflet of the cytoplasmic membrane, EMBO J. 15 (1996) 4239–4245.
[16] W.D. Stein, Kinetics of the P-glycoprotein, the multidrug transporter, Exp. Physiol. 83 (1998) 221–232.
[17] A.B. Shapiro, V. Ling, Extraction of Hoechst 33342 from the cytoplasmic leaflet of the plasma membrane by P-glycoprotein, Eur. J. Biochem. 250 (1997) 122–129.
[18] A.B. Shapiro, V. Ling, Stoichiometry of coupling of rhodamine 123 transport to ATP hydrolysis by P-glycoprotein, Eur. J. Biochem. 254 (1998) 189–193.
[19] D. Ferry, R. Boer, R. Callaghan, W.R. Ulrich, Localization of the 1, 4-dihydropyridine drug acceptor of P-glycoprotein to a cytoplasmic domain using a permanently charged derivative N-methyl dexniguldipine, Int. J. Clin. Pharmacol. Ther. 38 (2000) 130–140.
[20] Q. Qu, F.J. Sharom, Proximity of bound Hoechst 33342 to the ATPase catalytic sites places the drug binding site of P-glycoprotein within the cytoplasmic membrane leaflet, Biochemistry 41 (2002) 4744–4752.
[21] M.R. Lugo, F.J. Sharom, Interaction of LDS-751 with P-glycoprotein and mapping of the location of the R drug binding site, Biochemistry 44 (2005) 643–655.
[22] A.B. Shapiro, A.B. Corder, V. Ling, P-glycoprotein-mediated Hoechst 33342 transport out of the lipid bilayer, Eur. J. Biochem. 250 (1997) 115–121.
[23] H. Omote, M.K. Al-Shawi, A novel electron paramagnetic resonance approach to determine the mechanism of drug transport by P-glycoprotein, J. Biol. Chem. 277 (2002) 45688–45694.
[24] T.I. Orban, L. Seres, C. Ozvegy-Laczka, N.B. Elkind, B. Sarkadi, L. Homolya, Combined localization and real-time functional studies using a GFP-tagged ABCG2 multidrug transporter, Biochem. Biophys. Res. Commun. 367 (2008) 667–673.
[25] L. Homolya, Z. Hollo, M. Muller, E.B. Mechetner, B. Sarkadi, A new method for a quantitative assessment of P-glycoprotein-related multidrug resistance in tumour cells, Br. J. Cancer 73 (1996) 849–855.
[26] J.D. Allen, A. van Loevezijn, J.M. Lakhai, M. van der Valk, O. van Tellingen, G. Reid, J.H. Schellens, G.J. Koomen, A.H. Schinkel, Potent and specific inhibition of the breast cancer resistance protein multidrug transporter in vitro and in mouse intestine by a novel analogue of fumitremorgin C, Mol. Cancer Ther. 1 (2002) 417–425.
[27] A. Feofanov, S. Sharonov, I. Kudelina, F. Fleury, I. Nabiev, Localization and molecular interactions of mitoxantrone within living K562 cells as probed by confocal spectral imaging analysis, Biophys. J. 73 (1997) 3317–3327.
[28] L. Kaestner, Red blood cell ghosts and intact red blood cells as complementary models in photodynamic cell research, Bioelectrochemistry 62 (2004) 123–126.
[29] The Merck Index: an encyclopedia of chemicals, drugs, and biologicals, 14th edMerck & Co., Inc, Whitehouse Station, 2006.
[30] R. Regev, D. Yeheskely-Hayon, H. Katzir, G.D. Eytan, Transport of anthracyclines and mitoxantrone across membranes by a flip-flop mechanism, Biochem. Pharmacol. 70 (2005) 161–169.